Nanoflakes Hot Paper

DOI: 10.1002/anie.201404704

Hexagonal Transition-Metal Chalcogenide Nanoflakes with Pronounced Lateral Quantum Confinement**

Pere Miró, Jae Hyo Han, Jinwoo Cheon, and Thomas Heine**

Dedicated to Professor Gerhard Roewer on the occasion of his 75th birthday

Abstract: *Transition-metal chalcogenide (TMC) nanoflakes of composition MX_2 (where M = Ti, Zr and Hf; X = S and Se) crystallize preferentially in equilateral hexagons and exhibit a pronounced lateral quantum confinement. The hexagonal shape of octahedral (1T) TMC nanoflakes is the result of charge localization at the edges/vertices and the resulting Coulomb repulsion. Independent of their size, all nanoflakes have the M_nX_{2n-2} stoichiometry and thus an unoxidized metal center which results in dopant states. These states become relevant for small nanoflakes and lead to metallic character, but for larger nanoflakes (> 6 nm) the 2D monolayer properties dominate. Finally, coordination of Lewis bases at the nanoflake edges has no significant effect on the electronic structure of these species confirming the viability of colloidal synthetic approaches.*

The existence of two dimensional (2D) materials was a highly debated issue in solid-state physics concluding that these materials would be thermodynamically unstable at any finite temperature owing to thermal fluctuations.[1,2] The scientific community had to wait until last decade to disprove these statements and exfoliate graphite to graphene, the first 2D material to be isolated.[3,4] After this major scientific breakthrough, other layered materials, such as hexagonal boron nitride (*h*-BN), and transition-metal chalcogenides (TMCs) have been exfoliated down to monolayers.[5–7] Nowadays, 2D materials are a rapidly growing multidisciplinary field with a wide range of applications in nano- and optoelectronics, catalysis, and energy storage.[8] Transition-metal dichalcogenides are a prominent family of layered materials with the general formula of MX_2, where M is a transition metal and X is a chalcogen element. These materials are composed of 2D sheets stacked on top of one another. Each sheet is three atoms thick, with metal atoms in the middle, each of them covalently bound to the chalcogen atoms located above and below (Figure 1a). In the bulk and in stacked aggregates, TMC sheets are held together through interlayer London dispersion interactions. Nanostructures of layered TMCs are highly promising owing to their unique chemical and physical properties derived from the different nature of intra- and interlayer bonding. This provides a wide range of interesting anisotropic features for ion intercalation, spintronics, optoelectronics, and catalysis.[9–14] Furthermore, fascinating properties emerge when either the number of layers or the lateral system size is changed. For example, the exfoliation of bulk MoS_2 leads to photoluminescence at the monolayer level, while lateral confinement in WS_2 nanoflakes enhances its luminescence efficiency.[15–18] In this respect, the recent advances in the growth of TMC nanocrystals with a bottom-up synthetic approach have provided a route

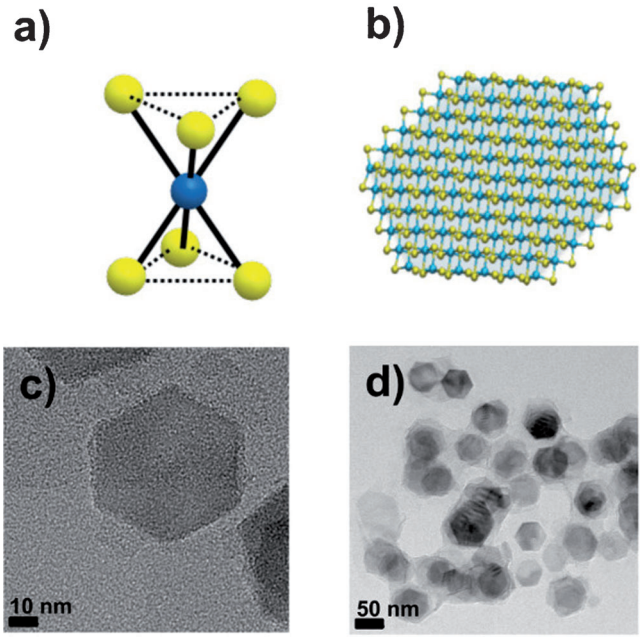

Figure 1. a) Visualization of basic atomic coordination of 1T-MX_2. b) atomic ball model of hexagonal shaped 2D transition-metal dichalcogenide nanoflake model with chemical composition of $Ti_{37}S_{72}$ (Ti_{37}^{Hex}) employed in this study. c) High- and d) low-magnification TEM images of synthesized hexagonal shaped TiS_2 nanoflakes. Transition metals blue, chalcogens yellow.

[*] Dr. P. Miró, Prof. Dr. T. Heine
School of Engineering and Science, Jacobs University Bremen
Campus Ring 1, 28759 Bremen (Germany)
E-mail: p.miro@jacobs-university.de
t.heine@jacobs-university.de
J. H. Han, Prof. Dr. J. Cheon
Department of Chemistry, Yonsei University
Seoul 120-749 (Korea)

[**] This work was supported by the German Research Council (Deutsche Forschungsgemeinschaft, HE 3543/18-1), The European Commission (FP7-PEOPLE-2009-IAPP QUASINANO, GA 251149 and FP7-PEOPLE-2012-ITN MoWSeS, GA 317451), The Office of Naval Research Global (N62909-13-1-N222), Air Force Office of Scientific Research (BAA-AFOSR-2013-0001-BRI-1), and the KRF Creative Research Initiative (2010-0018286) of Korea.

Supporting information for this article is available on the WWW under http://dx.doi.org/10.1002/anie.201404704.

towards true control on the nanoscale that has led to highly pure nanoflakes, produced at low-cost in a wide variety of chemical compositions, thicknesses, and sizes.[19–21] The synthesized nanocrystals are usually present in well-defined equilateral hexagonal shape. As an example, a synthesized 60 nm TiS_2 nanoflake is shown in Figure 1.

Herein, we report a study of the Group 4 1T-MX_2 TMCs (where M = Ti, Zr and Hf; X = S and Se) with the aim to understand the driving force behind the preferential nanoflake growing shape as well as the role of lateral quantum-confinement effects on both the electronic structure and properties of these species. We studied hexagonal and triangular shaped nanoflakes of increasing diameter following the M_n^Y nomenclature, where M is the transition metal, Y the shape (Hex = hexagonal, Tri = triangular, or Rho = rhomboid) and *n* the number of metal atoms in the nanoflake. The edges of 1T-TMC nanoflakes are well-defined with respect to other polytypes as a result of the octahedral coordination of the metal centers. Lateral confinement leads to the loss of one or two sulfur ligands at the edges and vertices of these species, respectively, giving square-pyramidal and tetrahedral coordination environments (Figure 2a). The number of metal atoms at the edges depends on the flake size and shape (if considering general six-sided figures), while the number vertices remains constant (six). All the nanoflakes have the M_nX_{2n-2} stoichiometry, independent of their chemical composition, size, or shape. In consequence, 1T-TMC nanoflakes have formally one metal center that is not oxidized, resulting in four electrons in excess with respect to the corresponding configuration in periodic 2D monolayers.

Our calculations reveal that the electrons in excess are analogous to n-doping in traditional semiconductors and located at the center of flakes. In Figure 2c (center), the electron density of the four excess electrons is presented for Ti_{37}^{hex} (see Figure S1–S12 and S20–S23 in the Supporting Information for other nanoflakes). The doping states are located at the center of the flake, but depleted for the edges and vertices. The electronic structure of small nanoflakes is better described as "metallic" at their center, while the edges retain the semiconductor electronic structure of the pristine 2D material. When increasing the flake size, the density of excess states at the "metallic" center reduces as it gets delocalized over a larger area for large nanoflakes. In analogy to semiconductor physics, if we define an effective gap excluding those "dopant states", Ti_{37}^{hex}, Zr_{37}^{hex}, and Hf_{37}^{hex} disulfides have electronic gaps of 0.82, 1.54, and 1.72 eV, respectively (Figure 2c left and right). On the other hand, their selenide analogues present significantly smaller gaps of 0.44, 0.99, and 1.15 eV, respectively.

Since the lateral confinement effects become negligible in larger flakes, we modeled them in respect to pristine 2D monolayers. Group 4 transition-metal disulfide monolayers are metallic for TiS_2 and semiconductors with indirect band gaps of 1.10 and 1.02 eV for ZrS_2 and HfS_2, respectively (Figure 3). There is a significant decrease in the band gap between Group 4 MS_2 and MSe_2 monolayers (see Figure S13–S15 and Table S1). These results are in excellent agreement with previous experimental and theoretical studies,[22,23] where an indirect band gap in the semiconducting materials originating from transitions from Γ to M high symmetry points on the Brillouin zone was reported (Figure 3). The 2D monolayer results reveal that lateral confinement in 1T-TMC nanoflakes induces a significant widening of the electronic band gaps. With increasing

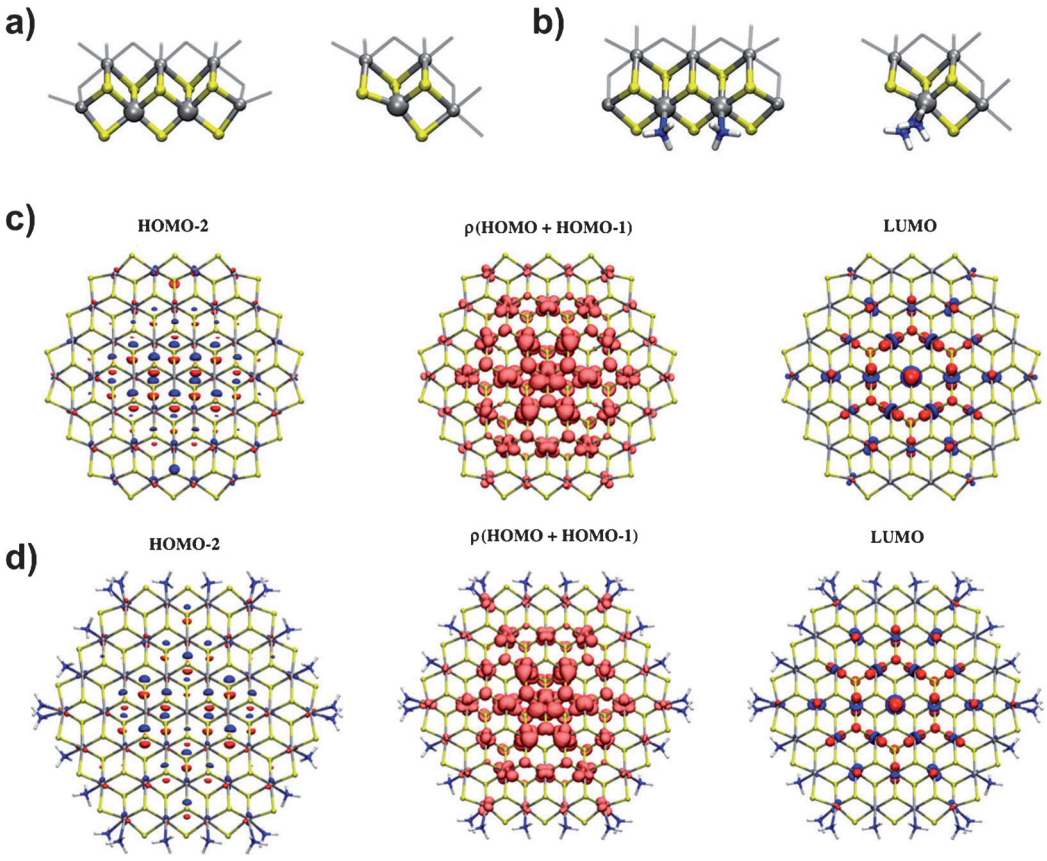

Figure 2. Crystal configuration of a) unsaturated b) and saturated nanoflakes edge and vertices. Ti gray, S yellow, N blue, H white, and extended nanoflake structure in semitransparent gray. c,d) Selected molecular orbitals and electron-density distributions for unsaturated (c) and saturated (d) Ti_{37}^{Hex} nanoflake. Isovalue 0.04.

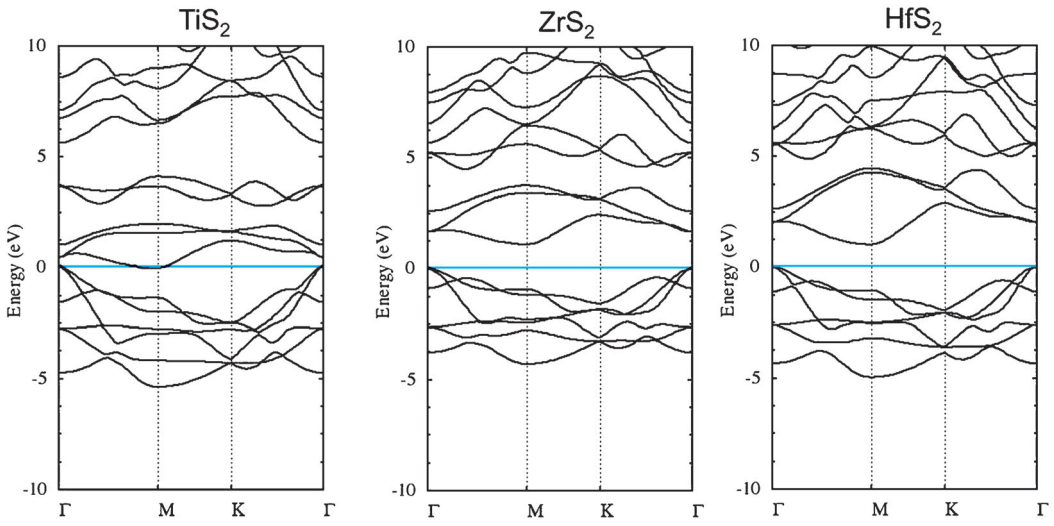

Figure 3. Band structure of 1T-TiS_2 (left), ZrS_2 (center), and HfS_2 (right) monolayers at the PBE level of theory. The Fermi level has been shifted to 0 eV and highlighted with a horizontal blue line.

nanoflake size the band gap approaches the bulk value. We estimate that the lateral confinement becomes negligible for TiS_2 systems with diameters larger than 6 nm with the loss of the gap (see Figure S16,S17 in the Supporting Information). This can be also observed in the evolution of the density of states (DoS) of TiS_2 nanoflakes, with the increase of the nanoflake size the DoS approaches the pristine TiS_2 monolayer value.

As observed in experiment, 1T-TMC nanoflakes are preferentially shaped as equilateral hexagons, however the driving force behind the high symmetry has not been explored to date. In a conventional model, electrostatics have been identified as the driving force behind the self-assembly and growth of many systems. Thus, we decided to study this possibility by performing a charge-distribution analysis on nanoflakes of different shapes (see Tables S2–S6 and Figure S18). The charge-distribution analyses for Ti_{37}^{hex} and Ti_{36}^{tri} nanoflakes presented in Figure 4 show that the partial charges at the vertices are significantly larger than those at the edges or in the basal planes (0.49, 0.32, and 0.14, respectively), which shows that electrostatic repulsion will occur through the charge accumulation at the vertices. In this regard, energy minimization takes place by the longest possible separation of the six vertices, with the resulting geometry being an equilateral hexagon that templates larger crystal shapes. This result is further supported by an energy decomposition of both Ti_n^{Hex} and Ti_n^{Tri} nanoflakes, where the total energy is assumed to be composed of contributions from metal sites of the basal plane (n_B), of the edges (n_E) and of the vertices (n_V): $E_{tot} = n_B E_B + n_E E_E + n_V E_V$. The analyses, detailed in Tables S7–S9 in the Supporting Information, converges rapidly to values of $E_B = -159.1$, $E_E = -158.9$, and $E_V = -136.3$ eV/unit, with the value for E_B correctly coinciding with the corresponding energy per MX_2 unit in the periodic monolayer. Since the number of vertices remains constant, independent of the nanoflake shape, these results indicate a higher stability of the geometrical arrangements with higher n_B/n_E ratio ($H > T$), thus confirming the preferred hexagonal shape of these species.

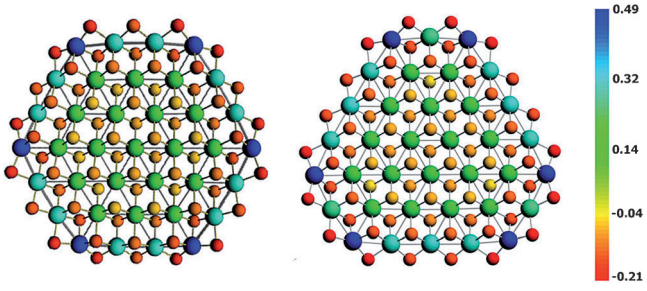

Figure 4. Partial atomic-charge distribution in Ti_{37}^{Hex} and Ti_{36}^{Tri} obtained from a multipole derived charge analysis (mdc-q).

Finally, the edges and vertices of 1T-TMC nanoflakes have been passivated with various surfactants, such as oleylamine as a stabilizer in colloidal synthesis. For this purpose we used structure models with ammonia as ligands at the vacant sites of the edges and vertices (Figure 2b). The coordination of these ligands did not impose significant changes on the electronic structure or properties of the nanoflakes confirming the viability of colloidal synthetic approaches (Figure 2d). In addition, the coordination of ammonia increases the positive partial charges of both edge and vertex metal atoms, which also favors the formation of hexagonal nanoflakes. Despite all of the research on these species, little is known about the strength and nature of the interaction of the amines with the edge 1T-TMC nanoflakes. To shed some light on this aspect, we studied the interaction of ammonia at the edge of M_{37}^{hex} nanoflakes. Ammonia strongly binds to the nanoflake edges with increasing coordination energy with increasing atomic number of the metal atom; −19.4, −25.3, and −25.0 kcal mol^{-1} per ammonia for Ti_{37}^{hex}, Zr_{37}^{hex}, and Hf_{37}^{hex} disulfide, respectively. Diselenides have comparable coordination energies and a similar trend (−19.1, −26.8 and −24.7 kcal mol^{-1} for titanium, zirconium, and hafnium diselenides, respectively), but no correlation is observed when comparing the sulfides and selenides. These bonding energies were decomposed using the Ziegler–Rauk method,[24] revealing an orbital contribution is on average five times larger than the electrostatic one, independent of the chemical composition of the nanoflake. Finally, we analyzed the topology of the electron density $\rho(r)$, finding a bond critical point (bcp) between the ammonia and the metal center ($\rho(r) > 0$, $\nabla\rho(r) =$

0, and $\nabla^2\rho(r) > 0$).[25] The use of more advanced density descriptors classifies these bonds as dative bonds, where the lone pair of the nitrogen atom is donated into the empty d orbitals of the metal center. This situation is further confirmed by the reduction of negative partial charge on nitrogen upon its coordination to the edges and vertices of the nanoflakes. No significant differences in bonding nature were found between edge and vertex coordinated ammonia (see Supporting Information for details).

In conclusion, our calculations demonstrate that Group 4 transition-metal 1T-TMC monolayers are indirect band gap semiconductors, except for TiS_2 and $TiSe_2$ which are metals. The lateral confinement significantly widens the electronic gap leading to semiconducting electronic structures, but the loss of the pristine stoichiometry induces dopant states. In small nanoflakes, these states are located at the center of the flakes where they become metallic, meanwhile the edges retain a semiconducting nature. In larger nanoflakes, the "dopant state" effects become negligible and the pristine 2D material's electronic structure is expected. The shape of the nanoflakes is determined by the following factors: despite maximization of the ratio of basal plane to edge atoms suggesting a circular shape, the extraordinary stability of one edge type and the Coulomb repulsion between the charged vertices impose the highest stability for equilateral hexagons. The coordination of Lewis bases at the edges indicates that a strong dative bond does not affect the electronic structure of these species, confirming the viability of colloidal synthetic approaches. Further studies are ongoing in our groups to extend the present study to stacks of nanoflakes (nanodiscs) and to other systems, such as noble 1T-TMC nanoflakes and other polytypes.

Experimental Section

Synthesis and characterization of 2D nanocrystals: The procedure presented in Ref. [20] was used to synthesize layered TMC nanocrystals with transition metals from Group 4. Using a standard hot-injection colloidal synthetic method, metal chloride precursors, and oleylamine as a co-surfactant and solvent are added to a three-neck round-bottom flask under Ar atmosphere. Then, the reaction mixture is first heated to 300 °C and CS_2 is injected rapidly into the reaction mixture. After the completion of reaction, excess butanol is added resulting precipitation of metal sulfide nanocrystals. The nanocrystals are washed with hexane and methanol (1:1) several times and characterized with TEM, XRD, and EDS.

Computational Details: Single-layer Group 4 TMC nanoflakes and their respective periodic 2D materials have been studied employing density functional theory (DFT). We have only considered the experimentally observed octahedral (1T) polytype (Figure 1 a), since there is no evidence of the existence of any other polytypes in contrast to other TMCs, such as MoS_2 or WS_2. All DFT calculations were performed using the Amsterdam Density Functional (ADF2013) program developed by Baerends, Ziegler, and co-workers.[26] We used the local VWN exchange-correlation potential with nonlocal dispersion corrected Perdew–Burke–Ernzerhof exchange-correlation functional (PBE-BJ-D3).[27–29] A triple- plus one polarization function basis set was used for all atoms. Relativistic corrections were introduced through the scalar zero-order regular approximation (ZORA).[30] For non-hydrogen atoms, the frozen-core approximation (small core) was used. Geometries were fully optimized taking advantage of symmetry when possible e.g. D_{3d} and C_{3v} for hexagonal and triangular nanoflakes, respectively. The topological analysis of the electron density was performed using the atoms in molecules (AIM) implementation in ADF2013. The amines used experimentally were modeled by ammonia to reduce both the computational time as well as to reduce the number of degrees of freedom in the edge and basal plane ligands.

Band structures of the pristine monolayers were calculated along the high symmetry points using the path Γ-M-K-Γ with the ADF2013-BAND package.[31] The band gap was evaluated on the PBE-BJ-D3 optimized structures. The layered structures were cut from the bulk structures in the direction of the layer stacking (001). Density Functional based Tight Binding (DFTB) calculations were performed using DFTB + program with the tiorg and mio parameter sets.[32–36] The DFTB molecular orbitals were plotted with Waveplot extension of DFTB + .

First principles calculations were used to study single-layered nanoflakes below 26 Å, while a tight binding approach was validated and used to study species up to 100 Å.

Received: April 25, 2014
Revised: July 10, 2014
Published online: September 11, 2014

Keywords: 2D materials · density functional theory · nanoflakes · quantum confinement · transition-metal chalcogenide

[1] E. M. Lifshitz, L. P. Pitaevskii in *Statistical Physics*, Part I & II, Pergamon, Oxford, **1980**.
[2] N. D. Mermin, H. Wagner, *Phys. Rev. Lett.* **1966**, *17*, 1133.
[3] K. S. Novoselov, A. K. Geim, S. V. Morozov, D. Jiang, Y. Zhang, S. V. Dubonos, I. V. Grigorieva, A. A. Firsov, *Science* **2004**, *306*, 666.
[4] K. S. Novoselov, A. K. Geim, S. V. Morozov, D. Jiang, M. I. Katsnelson, I. V. Grigorieva, S. V. Dubonos, A. A. Firsov, *Nature* **2005**, *438*, 197.
[5] A. Pakdel, Y. Bando, D. Golberg, *Chem. Soc. Rev.* **2014**, *43*, 934.
[6] R. Mas-Balleste, C. Gomez-Navarro, J. Gomez-Herrero, F. Zamora, *Nanoscale* **2011**, *3*, 20.
[7] V. Nicolosi, M. Chhowalla, M. G. Kanatzidis, M. S. Strano, J. N. Coleman, *Science* **2013**, *340*, 1420.
[8] P. Miró, M. Auddifred, T. Heine, *Chem. Soc. Rev.* **2014**, *43*, 6537.
[9] Q. H. Wang, K. Kalantar-Zadeh, A. Kis, J. N. Coleman, M. S. Strano, *Nat. Nanotechnol.* **2012**, *7*, 699.
[10] Y. G. Li, H. L. Wang, L. M. Xie, Y. Y. Liang, G. S. Hong, H. J. Dai, *J. Am. Chem. Soc.* **2011**, *133*, 7296.
[11] J. Xiao, D. Choi, L. Cosimbescu, P. Koech, J. Liu, J. P. Lemmon, *Chem. Mater.* **2010**, *22*, 4522.
[12] M. Chhowalla, H. S. Shin, G. Eda, L. J. Li, K. P. Loh, H. Zhang, *Nat. Chem.* **2013**, *5*, 263.
[13] Y. Wang, J. Z. Ou, S. Balendhran, A. F. Chrimes, M. Mortazavi, D. D. Yao, M. R. Field, K. Latham, V. Bansal, J. R. Friend, S. Zhuiykov, N. V. Medhekar, M. S. Strano, K. Kalantar-zadeh, *ACS Nano* **2013**, *7*, 10083.
[14] P. Miró, M. Ghorbani-Asl, T. Heine, *Angew. Chem. Int. Ed.* **2013**, *52*, 3015; *Angew. Chem.* **2013**, *125*, 3089.
[15] A. Kuc, N. Zibouche, T. Heine, *Phys. Rev. B* **2011**, *83*, 245213.
[16] K. F. Mak, C. Lee, J. Hone, J. Shan, T. F. Heinz, *Phys. Rev. Lett.* **2010**, *105*, 136805.
[17] A. Splendiani, L. Sun, Y. B. Zhang, T. S. Li, J. Kim, C. Y. Chim, G. Galli, F. Wang, *Nano Lett.* **2010**, *10*, 1271.
[18] L. Lin, Y. Xu, S. Zhang, I. M. Ross, A. C. M. Ong, D. A. Allwood, *ACS Nano* **2013**, *7*, 8214.
[19] J. H. Han, S. Lee, J. Cheon, *Chem. Soc. Rev.* **2013**, *42*, 2581.
[20] S. Jeong, D. Yoo, J. T. Jang, M. Kim, J. Cheon, *J. Am. Chem. Soc.* **2012**, *134*, 18233.

[21] S. Jeong, J. H. Han, J. T. Jang, J. W. Seo, J. G. Kim, J. Cheon, *J. Am. Chem. Soc.* **2011**, *133*, 14500.
[22] C. M. Fang, R. A. de Groot, C. Haas, *Phys. Rev. B* **1997**, *56*, 4455.
[23] A. Carvalho, R. M. Ribeiro, A. H. C. Neto, *Phys. Rev. B* **2013**, *88*, 115205.
[24] T. Ziegler, A. Rauk, *Inorg. Chem.* **1979**, *18*, 1755.
[25] R. F. W. Bader, *Atoms in Molecules. A Quantum Theory*, Oxford University Press, Oxford **1990**.
[26] ADF2013, SCM, Theoretical Chemistry, Vrije Universiteit, Amsterdam, The Netherlands, http://www.scm.com.
[27] J. P. Perdew, K. Burke, M. Ernzerhof, *Phys. Rev. Lett.* **1996**, *77*, 3865.
[28] J. P. Perdew, K. Burke, M. Ernzerhof, *Phys. Rev. Lett.* **1997**, *78*, 1396.
[29] S. Grimme, S. Ehrlich, L. Goerigk, *J. Comput. Chem.* **2011**, *32*, 1456.
[30] E. van Lenthe, E. J. Baerends, J. G. Snijders, *J. Chem. Phys.* **1993**, *99*, 4597.
[31] BAND2013, SCM, Theoretical Chemistry, Vrije Universiteit, Amsterdam, The Netherlands, http://www.scm.com.
[32] B. Aradi, B. Hourahine, T. Frauenheim, *J. Phys. Chem. A* **2007**, *111*, 5678.
[33] M. Elstner, D. Porezag, G. Jungnickel, J. Elsner, M. Haugk, T. Frauenheim, S. Suhai, G. Seifert, *Phys. Rev. B* **1998**, *58*, 7260.
[34] D. Porezag, T. Frauenheim, T. Köhler, G. Seifert, R. Kaschner, *Phys. Rev. B* **1995**, *51*, 12947.
[35] G. Seifert, D. Porezag, T. Frauenheim, *Int. J. Quantum Chem.* **1996**, *58*, 185.
[36] G. Dolgonos, B. Aradi, N. H. Moreira, T. Frauenheim, *J. Chem. Theory Comput.* **2010**, *6*, 266.

